Published in final edited form as:
Nanotechnology. 2008 July 15; 19(34): 1–10. doi:10.1088/0957-4484/19/34/345102.

Interaction between carbon nanotubes and mammalian cells: characterization by flow cytometry and application

Dong Cai[1,6], **Derek Blair**[1], **Fay J Dufort**[1], **Maria R Gumina**[1], **Zhongping Huang**[2], **George Hong**[3], **Dean Wagner**[4], **D Canahan**[2], **K Kempa**[5], **Z F Ren**[5], and **Thomas C Chiles**[1]

1 *Department of Biology, Boston College, Chestnut Hill, MA 02467, USA*

2 *NanoLab, Incorporated, Newton, MA 02458, USA*

3 *Bioprocess Division, Millipore Corporation, 80 Ashby Road, Bedford, MA 01730, USA*

4 *Naval Health Research Center, Detachment Environmental Health Effects Laboratory, Wright Patterson Air Force Base, OH 45433, USA*

5 *Department of Physics, Boston College, Chestnut Hill, MA 02467, USA*

Abstract

We show herein that CNT–cell complexes are formed in the presence of a magnetic field. The complexes were analyzed by flow cytometry as a quantitative method for monitoring the physical interactions between CNTs and cells. We observed an increase in side scattering signals, where the amplitude was proportional to the amount of CNTs that are associated with cells. Even after the formation of CNT–cell complexes, cell viability was not significantly decreased. The association between CNTs and cells was strong enough to be used for manipulating the complexes and thereby conducting cell separation with magnetic force. In addition, the CNT–cell complexes were also utilized to facilitate electroporation. We observed a time constant from CNT–cell complexes but not from cells alone, indicating a high level of pore formation in cell membranes. Experimentally, we achieved the expression of enhanced green fluorescence protein by using a low electroporation voltage after the formation of CNT–cell complexes. These results suggest that higher transfection efficiency, lower electroporation voltage, and miniaturized setup dimension of electroporation may be accomplished through the CNT strategy outlined herein.

1. Introduction

Magnetic nanomaterials, such as superparamagnetic nanoparticles (MNP), are gaining attention in biomedical applications from cell biology to clinical diagnosis and therapy [1,2] because of the convenience to control the interaction between MNP and cells [3] with magnetic forces. When MNP associate with cell membranes, intracellular organelles and molecules, the derivative complexes can be moved by magnetic force in a directed fashion [4,5]. Plasmid-attached MNP can concentrate plasmid DNA on cell surface under a magnetic field, thereby enhancing the plasmids access to cellular internalization pathways and consequently improving the transfection [6]. Another promising application of MNPs is the magnetically assisted separation of biomolecules and cells, and the removal of environmental pollutants [7,8]. Similarly, magnetic nanotubes can be made multifunctional with respect to separation, immunobinding, and drug delivery [9]. MNPs can generate hyperthermia in tumors when exposed to high-frequency electromagnetic field [10,11]. In the clinic, MNPs have been used

6Address for correspondence: Biology Department, Boston College, 414 Higgins Hall, Chestnut Hill, MA 02467, USA, E-mail: E-mail: caid@bc.edu.

as a contrast enhancing reagent for magnetic resonance imaging (MRI) by improving the proton relaxation. MNPs also allow efficient detection of gene expression *in vivo* [12,13].

Carbon nanotube (CNT) as a counterpart of the nanoparticle in biomedical applications offers promising performance in biomolecule delivery [14] and anti-cancer therapy [15]. The surface chemistry of CNT enables efficient molecule loading and effective biocompatible modifications [16,17]. Different mechanisms have been employed to mediate the interaction between CNT and cells. CNTs decorated with macromolecules or functionalized with small groups can be readily internalized by cells [18,19]. The high aspect ratio and electrical conductivity of CNT has been exploited to enhance the electric field, thereby facilitating the electroporation, a long-standing transfection technique based on the phenomenon of cell membrane permeabilization under electric field [20]. The field-mediated CNT–cell interaction has also be used to drive CNTs by magnetic force to penetrate cell membranes and shuttle DNA payloads into the cells, by a process termed nanospearing [21]. The spear-making CNT are synthesized by plasma enhanced chemical vapor deposition (PECVD) process [22]. CNTs produced by PECVD have uniform and controllable morphology (i.e., length, diameter, and alignment). A metallic nanoparticle is always embedded in each CNT tip due to the special growth mechanism [23]. The as-grown magnetic nanoparticle can facilitate the actuation of CNT in magnetic field. The advantages of this one-dimensional conductive nanostructure exist in the ease of production, geometry adjustment and surface chemistry, as well as capability to enhance the electric field. So it holds potentials for a variety of biomedical applications such as biological sensing, molecular delivery, separation and purification.

Biomedical applications of nanomaterials usually require effective manipulation of the physical or chemical interactions between the nanostructures and biological cells, as well as efficient and quantitative characterizations of the interaction in live cells. Currently, the characterization is intensively relying on microscopy, which is difficult to generate an accurate and prompt overview of the interactions between nanomaterials and cells. The lack of information on the interaction also prevents people from optimization of nanomaterial facilitated biotechniques.

In this paper, we used a magnetic field to associate the CNTs to Bal17 and primary B cells to the CNTs. Flow cytometry was utilized to quantitatively characterize the magnetic association between CNTs and cells. The side scattering signal (SSC) level was proportional to the amount of CNTs that were complexed with the cells. The phenomenon was compared in cell line and non-dividing primary cells. Cell viability and apoptosis assays were conducted to evaluate the compatibility of the treatments to cells. The strength of the association between CNTs and cells was demonstrated in cell separation with magnetic force. In addition, the CNT–cell complexes were also utilized to facilitate electroporation due to the electric field enhancement by the CNT as a conductive one-dimensional nanostructure.

The complex was also examined through the magnetically mediated cell separation. Due to the ideal one-dimensional conductive structure, this kind of CNT can enhance the electric field at both ends. The potential to use CNTs to facilitate electroporation was demonstrated by the reduced time constant and enhanced green fluorescence protein (EGFP) transfection in the mammalian cells.

2. Experimental details

2.1. Carbon nanotube preparation

A silicon wafer was coated with chromium and nickel layers of 350 and 30 nm, respectively. The nanotubes were grown in a hot filament PECVD system [21,23]. A base pressure of 10^{-6} Torr was used before the introduction of acetylene and ammonia gases. The growth

pressure was 10–20 Torr, and the growth time was 1–10 min for proper nanotube length control. The substrate temperature was maintained below 660 °C. The nanotubes were lifted off the silicon wafer by sonication in ethyl alcohol to make the stock suspension. Such a stock can be keep on shelf for months. Alternatively, stock suspension was made by resuspending the nanotubes in phosphate buffered saline (PBS) following centrifugation at 10 000 g at room temperature for 10 min. No noticeable difference in the performance was observed between the two preparations.

There are different approaches to estimate the CNT concentration. The one we take is to use the SEM image and get the rough reading of the amount of CNTs on a randomly picked area of CNT chip as shown in figure 1(a). The length of a nanotube marked by arrow is 1 μm. The white-lined square covers an area of 2 μm × 2 μm that contains 126 nanotubes. Therefore, the total amount of CNTs and the concentration can be directly converted to mole and molarity. We concentrated CNT suspension by centrifugation and drying the CNT pellet in a vacuum desiccator. The weight of CNT was obtained with AT261 delta range balance (Mettler-Toledo International Inc., Columbus, OH). Correspondingly, 20 fmol (according to previous estimation) CNT obtained from 10 ml suspension is about 168 μg. On average, the CNT used in our experiment was 1 μm in length and 100 nm in diameter. Since the graphite and single walled CNT density are 1.7 and 1.33 g cm^{-3} respectively, we assume the multi walled CNT used here has the density of 1.5 g cm^{-3}. Then, each CNT has a mass of 11.8 fg. Correspondingly, 168 μg CNT is about 23 fmol.

2.2. CNT poly-L-lysine complex (PLL–CNT) formation

CNTs were first functionalized with carboxyl groups as described before [21]. Then they were suspended in 1 ml 0.1 M 2-[N-morpholino]ethane sulfonic acid (MES) buffer (pH 4.5) containing 10 μl 0.01% poly-L-lysine (PLL, 70 kD to 140 kD) (Sigma-Aldrich) and 10 mg 1-ethyl-3-(3-dimethylaminopropyl) carbodiimide (EDC) (Sigma-Aldrich) to couple the primary amine groups in the PLL molecules to the carboxylic groups on carbon nanotubes. PLL–CNT complexes were formed after incubation in dark at room temperature for 1 h.

The complexes were washed four times with 1 ml PBS. The final dispersion was made in complete RPMI-1640 culture medium.

2.3. Cell preparation

BALB/cByJ mice were purchased from The Jackson Laboratories (Bar Harbor, ME). The mice were cared for and handled at all times in accordance with National Institutes of Health and Boston College guidelines. Splenic B cells were purified by depletion of T cells with anti-Thy-1.2 plus rabbit complement; macrophages (and other adherent cells) were removed by plastic adherence [24]. Red blood cells and non-viable cells were removed by sedimentation on Lympholyte-M gradients (Accurate Chemical and Scientific Co., Westbury, MA). The resulting B cells were then centrifuged through discontinuous Percoll gradients in order to isolate quiescent (naïve) B cells [25]. The cells were then cultured in RPMI-1640 medium supplemented with 10 mM HEPES (pH 7.5), 2 mM L-glutamine, 50 μM β-mercaptoethanol, 100 U ml^{-1} penicillin, 100 μg ml^{-1} streptomycin, 0.25 μg ml^{-1} amphotericin B and 10% heat-inactivated fetal bovine serum (Atlanta Biologicals, Lawrenceville, GA). B cells were cultured at 3×10^6 cells ml^{-1} in a water-jacketed CO_2 incubator.

Bal17 B-lymphoma cells were cultured in RPMI 1640 medium supplemented as above with 5% heat-inactivated fetal calf serum at 1×10^6 cells ml^{-1} in the incubator.

2.4. Flow cytometry

We used a BD FACSCanto flow cytometer (BD Bioscience, San Jose, CA). The data were acquired and analyzed with BD FACSDiva software. Cells were suspended at 5×10^4 ml^{-1} prior to acquisition. A blank sample was first used as a reference for adjusting controlling voltages of FSC, SSC and other channels such as propidium iodide (PI), Annexin V-Cy-5 and green fluorescence (GFP). To evaluate cell death and apoptosis, the speared B cells were incubated in 1 ml staining solution containing Annexin V-Cy-5 (5 μg ml^{-1}) and propidium iodide (10 μg ml^{-1}) for 5 min. The leaky membrane of a dying cell allowed the positively charged PI molecules to enter and stain the cell by intercalating double stranded DNA in nucleus. Upon excitation with laser of 488 nm, the PI stained cells can emit fluorescence at 617 nm and produce signals in the corresponding recording channel of the flow cytometer. In apoptotic cells, Annexin V can bind to phosphatidyl serine which flips to the outer surface of the cell membrane. The excitation and emission wavelength maxima of Cy-5 are 650 nm and 670 nm respectively.

2.5. Magnetic CNT and cell association

Two hours before the experiment, the cells were dispersed in a 12-well plate at 1×10^6/well and 3×10^5/well for primary splenic B cell and Bal17 cells respectively. The cell culture medium was replaced by 1 ml CNT suspension for each well. After the plate was placed on a Nd–Fe–B permanent magnet for 5–20 min, the cells were resuspended in new culture medium and washed twice with PBS. To separate the CNT associated cells from the non-associated cells, the magnet was put beside the 1.5 ml centrifuge tube containing the cells. It required 10–20 min to attract the CNT associated cells to the sidewall. After the separation, the supernatant became clear indicating very few CNT associated cells inside. The supernatant was extracted and marked as ‘clear part’; the dark pellet on the sidewall was resuspended as ‘dark part’ with equal volume of PBS as ‘clear part’. Then the samples were analyzed with flow cytometer.

2.6. Electroporation

Each electroporation cuvette (cooled on ice) was loaded with 3×10^6 regular or CNT associated Bal17 cells in suspension adjusted to 200 μl. A Gene Pulser electroporation system (BIO-RAD, Hercules, CA) was High Cap, 960 μF. Voltages were selected from 100 to 250 V. For the transfection experiments, pEGFP plasmid DNA (Clontech, Mountain View, CA) was supplemented to the cell suspensions in the cuvettes. After the electroporation, the cells were placed on ice for 5 min and then dispersed in a 6-well plate with 2 ml complete culture medium. The cells were checked with flow cytometer 48 h later.

3. Results and discussion

CNTs were grown on a silicon substrate. According to scanning electronic microscopy (SEM) of the nanotube array (figure 1(a)), the on-chip CNT amount was estimated. CNTs from a 2 cm × 2 cm chip were then placed into 5 ml ethanol to make ~4 pM suspension. If the container was placed beside a Nd–Fe–B magnet, the nanotubes were collected on the sidewall by the magnetic force (figure 1(b)).

To start experiments, the stock CNT suspension was briefly sonicated and resuspended in fetal bovine serum (FBS) supplemented RPMI-1640 cell culture medium. The protein components in FBS such as albumin can non-specifically attach to the CNT [26], thereby allowing CNTs to remain in solution for more than 1 h. UV–vis spectrometry was used to evaluate the amount of nanotubes suspended in RPMI1640 with FBS. CNT samples were observed with UV–vis spectrometry immediately after sonication, in order to obtain standard charts, as shown in figure 1(c). The characteristic signal of our CNT was observed at 450–600 nm. The absorbance at λ_{460} was used to indicate CNT concentration. After sitting for 2 h, the sample containing 2 pM

was centrifuged at 2000 g for 5 min to remove aggregated large CNT clusters. Then the supernatants were measured again. More than 95% of the CNT remained stably in serum supplemented suspension.

Nanospearing molecular delivery [21] was used to associate CNTs with cells by a magnetic field. As shown in scheme 1, CNTs in suspension can be directed down to the bottom following the magnetic field lines. If there are cells dispersed on the bottom in advance, the CNTs will stop on the cell surface and then be driven by the magnetic force to attach or even penetrate the cell membranes; we anticipate the association between the CNTs and cells will be strong enough to support the physical manipulations such as physical resuspension and separation with magnetic field. The Bal17 cells treated with CNT in the presence and absence of magnetic forces were inspected by microscopy in figure 2 together with the comparison of CNT dosages. No obvious CNT–cell association was observed without magnetic field. Other characterizations of the association were carried out with scanning electron microscopy and confocal microscopy in our previous reports [21,27].

Flow cytometry allows a large number of cells to be analyzed individually. Basically, a single wavelength laser beam illuminates each cell and generates forward scatter signal (FSC), side scatter signal (SSC). FSC correlates with cross-sectional area of a cell and SSC depends on the intracellular complexity of the cell such as the membrane roughness, the shape of nucleus, and the amount of cytoplasmic granules. Hypothetically, the presence of CNTs on cell membranes can alter laser scattering signals, which should be quantitatively measured by flow cytometry. We therefore used flow cytometry to quantitatively measure the level of CNTs and cells association, as illustrated in scheme 1.

The nanospeared primary B cells generated distinctive SSC pattern (figure 3(a)). Normal viable cells have lower SSC and higher FSC compared to dying cells or cell debris. The normal cell population can be gated in the SSC–FSC scatter plot, as shown in the control data. The FSC and SSC histograms of the gated population are displayed separately. Upon association with CNTs, a larger cellular SSC was observed, while the level of FSC and percentage of normal cells remained the same as control (i.e., non-speared cells). Both primary B cells and Bal17 cells exhibited CNT induced SSC increases. The difference was that the enhanced SSC persisted for several days in primary B cells, while the enhanced SSC was lost by 24 h in Bal17 cells (figure 3(b)) indicating dissociation with CNTs. This may reflect the continuous turn-over of the Bal17 cell plasma membrane with each division. On the contrary, primary B cells do not divide in the absence of growth factors [27]. The primary B cell membranes remained stable and maintained the CNT–cell complexes.

We also investigated the effects of spearing periods and amount of CNT on the SSC. In figure 4(a), 0.4 mol CNTs increased SSC from 19 000 to 39 000 units, while changing the spearing period from 5 to 20 min produced no significant change, suggesting that 5 min was sufficient to allow association of CNTs with the cell surface. This time is determined by parameters such as magnetic field gradient, buffer volume, dimensions of the CNTs, solution viscosity and membrane fluidity in our nanospearing setup. We initially used PLL–CNT to study the CNT and cell association. However, when it was compared with PLL-free CNT, we noticed that PLL–CNT induced the same level of SSC at the concentration as low as one fourth of the latter (figure 4(b)), suggesting that PLL–CNT had higher potency than regular CNT to associate to cell membrane and enhance the SSC. A plausible explanation was that the electrostatic attraction between the counter charges carried by the PLL–CNT and the cell membranes facilitated the formation of CNT–cell complexes.

The PLL–CNTs were used to demonstrate the SSC responses with respect to the CNT dosage up to 6.4 fmol. In parallel, the cells were stained with propidium iodide (PI) to monitor the cell

viability by flow cytometry. In figure 5(a), the viable splenic B cell population in SSC–FSC plot was marked in green according to the PI positive gate in the histogram. The nanospeared cell viability remained at a similar level despite a high SSC level that was saturated when 6.4 fmol CNTs were used for nanospearing (figure 5(b)). Of note, the CNT tended to precipitate and formed clusters at high concentration. This led to the reduction of spearing efficiency and might be the reason that SSC decreased 6.4 fmol.

We also investigated apoptosis, which may be triggered by the CNT association in the cells. CNT suspensions in 400 μl containing 0.2, 0.8 and 2.4 fmol respectively were applied onto Bal17 cells. The cells without CNTs were taken as the control. The apoptosis assay was conducted after cell incubation for 2 and 24 h. As shown in figure 6, no apparent changes in the percentage of Annexin positive cells (Q2 + Q4) were observed corresponding to the CNT dosages as well as with respect to the incubation time. For Q1 and Q3, the percentages correspond to 0.5 and 95%, respectively, regardless of the concentration of CNTs used. The result indicated that CNT association does not produce additional programed cell death.

Following the magnetic separation of the speared cells, we obtained ‘dark part’ and ‘clear part’ suspension samples following the procedures in section 2. The samples contained cells with and without CNTs, respectively. The SSC of the two parts exhibited significant difference. For the dark part, the SSC increased to 15×10^4, while the clear part exhibited SSC under 3×10^4 (figure 7(a)). The cell counts in both parts were normalized to the total amount of cells. As shown in figure 7(b), the cells were magnetically collected into the dark part at a percentage depending on the amount of CNTs associated with cells. For example, at 1.6 fmol, more than 90% of the cells were in complexes with CNTs. The complex structure remained stable during the process to support the physical handling of cells.

CNTs are usually considered as 1D conductive structures. The electric field enhancement at their tips was utilized for improving electroporation [20]. The field enhancement coefficient is a function of the distance to CNT tips (figure 8(a), inset table). Provided that the CNT is 1 μm long and 100 nm thick, the electric fields (E) nearly at the tips will be 33.5-fold of the applied electric field (E_0). However, at a 200 nm distance from the tips, the electric fields only have 0.6-fold enhancement. Thereafter, the efficiency of electroporation largely depends on the proximity of the cell membrane to the CNT tips. Moreover, the electroporation will be enhanced by using the method address above to associate CNTs to cell membranes prior to applying the electric field. The close contact between CNTs and cell membranes will guarantee the poration of membranes with the highly enhanced field by CNTs.

A general indicator of electroporation is the transient time constant at the decaying phase when an electric pulse is used to generate the field. It is correlated to the permeability of cell membrane as the result of electroporation. The extra and intracellular molecular (or ionic) exchange can lead to increase of the ionic strength and decrease of the dielectric constant. The corresponding reduction of resistance and capacitance result in smaller time constant. Thus, the time constant is inversely proportional to the level of electroporation.

We used Bal17 cells to test nanotube-facilitated electroporation since the lymphoma cells are more amenable to transfection than the primary B cells. The time constants corresponding to cells without CNTs and CNT associated cells were plotted versus voltages in figure 8(b). Clearly, the time constant decreased in CNT associated cells comparing to CNT-free Bal17 cells. The time constant of CNT associated cells at 150 V was 58 ms. The value was comparable to the time constant obtained from CNT-free cells at 230 V, which was the voltage we can obtain transfection in the CNT-free cells. The transfection was carried out by adding pEGFP plasmid to the cell suspension in the cuvette. We checked the transfection results 48 h after the electroporation by flow cytometry. As shown in figure 8(c), CNT associated cells demonstrated

improvement in the EGFP transfection in terms of the percentage of EGFP positive cells and the average amplitudes of EGFP signals in comparison to the control cells electroporated without the plasmid, cells.

The results of CNT facilitated electroporation suggest that magnetic CNT may be used to improve electroporation with the following advantages: (1) the magnetic association between the cells and CNTs can bring the cell membranes and CNT tips in close contact to optimally facilitate the electroporation; (2) the metal particles located inside the CNTs can provide more free electrons at the tip to afford higher enhancement of the electric field; (3) the consistency of CNT length and aspect ratio allow quantitative control and adjustment of the electroporation strength. Such advantages hold promise for the enhancement of the electroporation upon optimization of the parameters, such as amount of CNTs, level of CNT association to cells, buffer contents, pulse waveform and cuvette size.

4. Conclusion

We show herein that magnetically drivable CNTs can form complexes with cells in the presence of a magnetic field. The complexes can be analyzed by flow cytometry based on the discovery of the relationship between CNT–cell association and the SSC. The amplitude of SSC is proportional to the amount of CNTs that are associated with cells. In contrast to undividing primary B cells, dividable Bal17 cells associated to CNTs can recover the regular SSC level of normal cells overnight due to the membrane turnover. This indicates the loss of CNT association on the cell surface. Immediately after the association between CNTs and cells, the complexes are strong enough to be magnetically manipulated and separated with magnetic force. The cell viability and levels of apoptosis and necrosis under the applicable high CNT concentration remain the same as the CNT-free cells giving support to the biomedical applications of the CNT–cell association process. The CNT–cell complexes can be utilized to facilitate electroporation. A high level of pore formation in cell membranes is indicated by the reduced electroporation time constant in CNT–cell complexes. The expression of enhanced green fluorescence protein can be achieved with a low electroporation voltage in the CNT associated cells. These results suggest a feasible approach to achieve efficient electroporation with mild electrical conditions.

Briefly, our research demonstrates a practical method to magnetically manipulate mammalian cells with nanomaterials as well as the quantitative assessment of the interaction between live cells and nanomaterials, and shows a promising method for efficient molecular delivery.

A majority of nano-biotechnology applications comprise direct interactions between nanomaterials and biological cells correlated to receptor binding, antigen–antibody recognition, and internalization. Flow cytometry is an established tool in cell biology research and herein has revealed new values in nano-biotechnology. The change in laser scattering signals can be observed once the nanomaterials associated with the cell membranes. Emerging concerns about nanomaterial toxicity and biocompatibility extended the corresponding cell biology and immunology interests to the subcellular structures and signal transduction pathways [28–31]. It is foreseeable that the presence of nanomaterials in the subcellular apparatuses will be indicated by SSC, so that the interaction can be rapidly and quantitatively evaluated. The information obtained can provide invaluable reference to monitor and optimize the processes in biomedical applications of nanomaterials.

Acknowledgements

We thank NIBIB of NIH (1R43EB006249-01A1)(DC), Naval Health Research Center/Environmental Health Effects Lab of Department of Navy (FA8601-07-P-0548) (DC and TCC);DOE(DE-FG02-00ER45805)(ZFR) and NSF(NIRT

0506830)(ZFR) for supporting the research. We also thank Dr Peter Bartholomew for help with electroporation experiments.

The views expressed are those of the authors and do not reflect the official policy or position of the Department of the Navy, Department of Defense, or the US Government.

References

1. Pankhurst QA, Connolly J, Jones SK, Dobson J. Applications of magnetic nanoparticles in biomedicine. J Phys D: Appl Phys 2003;36:R167.
2. Schutt W, Gruttner C, Hafeli U, Zborowski M, Teller J, Putzar H, Schumichen C. Applications of magnetic targeting in diagnosis therapyspossibilities limitations: a mini-review. Hybridoma 1997;16:109. [PubMed: 9085137]
3. Wilhelm C, Gazeau F, Roger J, Pons JN, Bacri JC. Interaction of anionic superparamagnetic nanoparticles with cells: kinetic analyses of membrane adsorption subsequent internalization. Langmuir 2002;18:8148.
4. Bausch AR, Ziemann F, Boulbitch AA, Jacobson K, Sackmann E. Measurement of local viscoelasticity forces in living cells by magnetic tweezers. Biophys J 1999;76:573. [PubMed: 9876170]
5. Won J, Kim M, Yi YW, Kim YH, Jung N, Kim TK. A magnetic nanoprobe technology for detecting molecular interactions in live cells. Science 2005;309:121. [PubMed: 15994554]
6. Scherer F, Anton M, Schillinger U, Henke J, Bergemann C, Krüger A, Gänsbacher B, Plank C. Magnetofection: enhancing targeting gene delivery by magnetic force *in vitro* and. in vivo Gene Ther 2002;9:102.
7. Bergemann C, Muller-Schulte D, Oster J, Brassard L, Lubbe AS. Magnetic ion-exchange nano- microparticles for medical biochemical molecular biological applications. J Magn Magn Mater 1999;194:45.
8. Nunez L, Kaminski MD. Transuranic separation using organophosphorus extractants adsorbed onto superparamagnetic carriers. J Magn Magn Mater 1999;194:102.
9. Son JS, Jonathan R, He B, Schuchman M, Lee SB. Magnetic nanotubes for magnetic-field-assisted bioseparation biointeraction drug delivery. J Am Chem Soc 2005;127:7316. [PubMed: 15898772]
10. Jordan A, Scholz R, Wust P, Fahling H, Krause J, Wlodarczyk W, Sander B, Vogl T, Felix R. Effects of magnetic fluid hyperthermia (MFH) on C_3H mammary carcinoma *in vivo*. Int J Hyperth 1997;13:587.
11. Ito A, Shinkai M, Honda H, Kobayashi T. Heat-inducible TNF-alpha gene therapy combined with hyperthermia using magnetic nanoparticles as a novel tumor-targeted therapy. Cancer Gene Ther 2001;8:649. [PubMed: 11593333]
12. Hogemann D, Josephson L, Weissleder R, Basilion JP. Improvement of MRI probes to allow efficient detection of gene expression. Bioconjug Chem 2000;11:941. [PubMed: 11087345]
13. Weissleder R, Moore A, Mahmood U, Bhorade R, Benveniste H, Chiocca EA, Basilion JP. *In vivo* magnetic resonance imaging of transgene expression. Nat Med 2000;6:351. [PubMed: 10700241]
14. Bianco A. Carbon nanotubes for the delivery of therapeutic molecules. Expert Opin Drug Deliv 2004;1:57. [PubMed: 16296720]
15. Kam NW, O'Connell M, Wisdom JA, Dai H. Carbon nanotubes as multifunctional biological transporters near-infrared agents for selective cancer cell destruction. Proc Natl Acad Sci USA 2005;102:11600. [PubMed: 16087878]
16. Singh R, Pantarotto D, Lacerda L, Pastorin G, Klumpp C, Prato M, Bianco A, Kostarelos K. Tissue biodistribution blood clearance rates of intravenously administered carbon nanotube radiotracers. Proc Natl Acad Sci USA 2006;103:3357. [PubMed: 16492781]
17. Kam NW, Chen RJ, Li Y, Dai H. Functionalization of carbon nanotubes for biocompatibility biomolecular recognition. Nano Lett 2002;2:285.
18. Kam NW, Jessop TC, Wender PA, Dai H. Nanotube molecular transporters: internalization of carbon nanotube–protein conjugates into mammalian cells. J Am Chem Soc 2004;126:6850. [PubMed: 15174838]
19. Pantarotto D, Briand JP, Prato M, Bianco A. Translocation of bioactive peptides across cell membranes by carbon nanotubes. Chem Commun 2004:16.

20. Rojas-Chapana J, Troszczynska J, Firkowska I, Morsczeck C, Giersig M. Multi-walled carbon nanotubes for plasmid delivery into *Escherichia coli* cells. Lab Chip 2005;5:536. [PubMed: 15856091]
21. Cai D, Mataraza JM, Qin ZH, Huang Z, Huang J, Chiles TC, Carnahan D, Kempa K, Ren Z. Highly efficient molecular delivery into mammalian cells using carbon nanotube spearing. Nat Methods 2005;2:449. [PubMed: 15908924]
22. Ren ZF, Huang ZP, Xu JW, Wang JH, Bush P, Siegal MP, Provencio PN. Synthesis of large arrays of well-aligned carbon nanotubes on glass. Science 1998;282:1105. [PubMed: 9804545]
23. Wen JG, Huang ZP, Wang DZ, Chen JH, Yang SX, Ren ZF, Wang JH, Calvet LE, Chen J, Klemic JF, Reed MA. Growth and characterization of aligned carbon nanotubes from patterned nickel nanodots and uniform thin films. J Mater Res 2001;16:3246.
24. Doughty CA, Bleiman BF, Wagner DJ, Dufort FJ, Mataraza JM, Roberts MF, Chiles TC. Antigen receptor-mediated changes in glucose metabolism in B lymphocytes: role of phosphatidylinositol 3-kinase signaling in the glycolytic control of growth. Blood 2006;107:4458. [PubMed: 16449529]
25. Hodgkin PD, Yamashita LC, Coffman RL, Kehry MR. Separation of events mediating B cell proliferation Ig production by using T cell membranes lymphokines. J Immunol 1990;145:2025. [PubMed: 2144543]
26. Chen RJ, Bangsaruntip S, Drouvalakis KA, Kam NW, Shim M, Li Y, Kim W, Utz PJ, Dai H. Noncovalent functionalization of carbon nanotubes for highly specific electronic biosensors. Proc Natl Acad Sci USA 2003;100:4984. [PubMed: 12697899]
27. Cai D, Doughty CA, Potocky TB, Dufort FJ, Huang Z, Blair D, Kempa K, Ren ZF, Chiles TC. Carbon nanotube-mediated delivery of nucleic acids does not result in non-specific activation of B lymphocytes. Nanotechnology 2007;18:365101.
28. Lam CW, James JT, McCluskey R, Arepalli S, Hunter RL. A review of carbon nanotube toxicity assessment of potential occupational environmental health risks. Crit Rev Toxicol 2006;36:189. [PubMed: 16686422]
29. Manna SK, Sarkar S, Barr J, Wise K, Barrera EV, Jejelowo O, Rice-Ficht AC, Ramesh GT. Single-walled carbon nanotube induces oxidative stress activates nuclear transcription factor—kappaB in human keratinocytes. Nano Lett 2005;5:1676. [PubMed: 16159204]
30. Dumortier H, Lacotte S, Pastorin G, Marega R, Wu W, Bonifazi D, Briand JP, Proato M, Muller S, Bianco A. Functionalized carbon nanotubes are non-cytotoxic preserve the functionality of primary immune cells. Nano Lett 2006;6:1522. [PubMed: 16834443]
31. Chithrani BD, Ghazani AA, Chan WCW. Determining the size shape dependence of gold nanoparticle uptake into mammalian cells. Nano Lett 2006;6:662. [PubMed: 16608261]

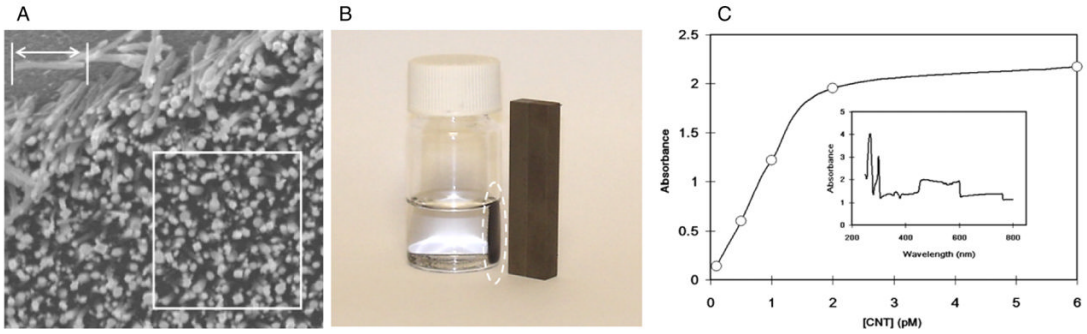

Figure 1.

(a) Carbon nanotube array grown by plasma enhanced chemical vapor deposition. The length of a nanotube marked by arrow is 1 μm. The white-lined square covers an area of 2 μm × 2 μm that contains 126 nanotubes. (b) Carbon nanotubes collected on the sidewall by a magnet. (c) UV–vis measurement of carbon nanotube suspensions in culture medium. The absorbance values at λ_{460} is correlated to the concentration of CNTs. The inset is a typical spectrum of CNT at 4 pM scanning from 190 to 800 nm.

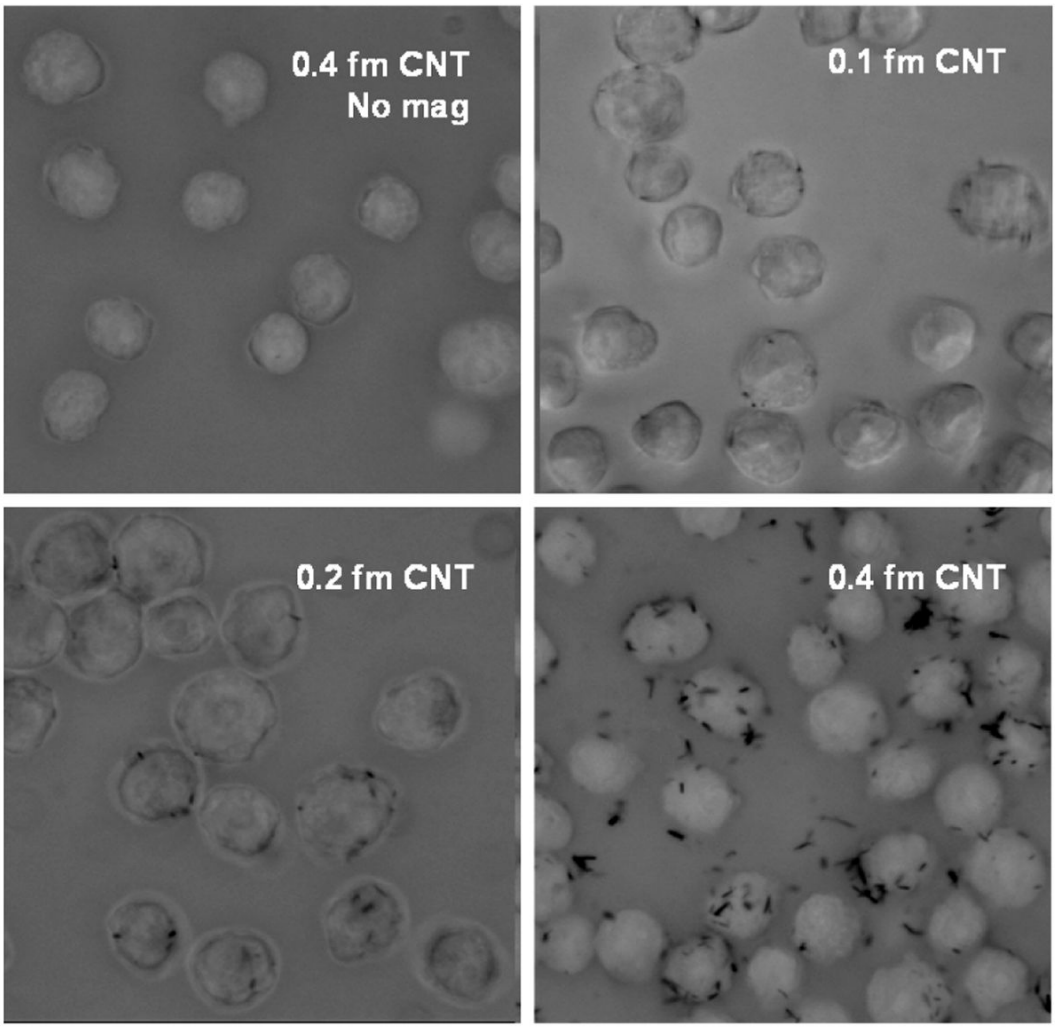

Figure 2.
Bal17 cells associated with different amount of CNTs. The cells were pipetted several times to remove the non-associated CNTs. The CNTs bundled together appeared as black dots in cells.

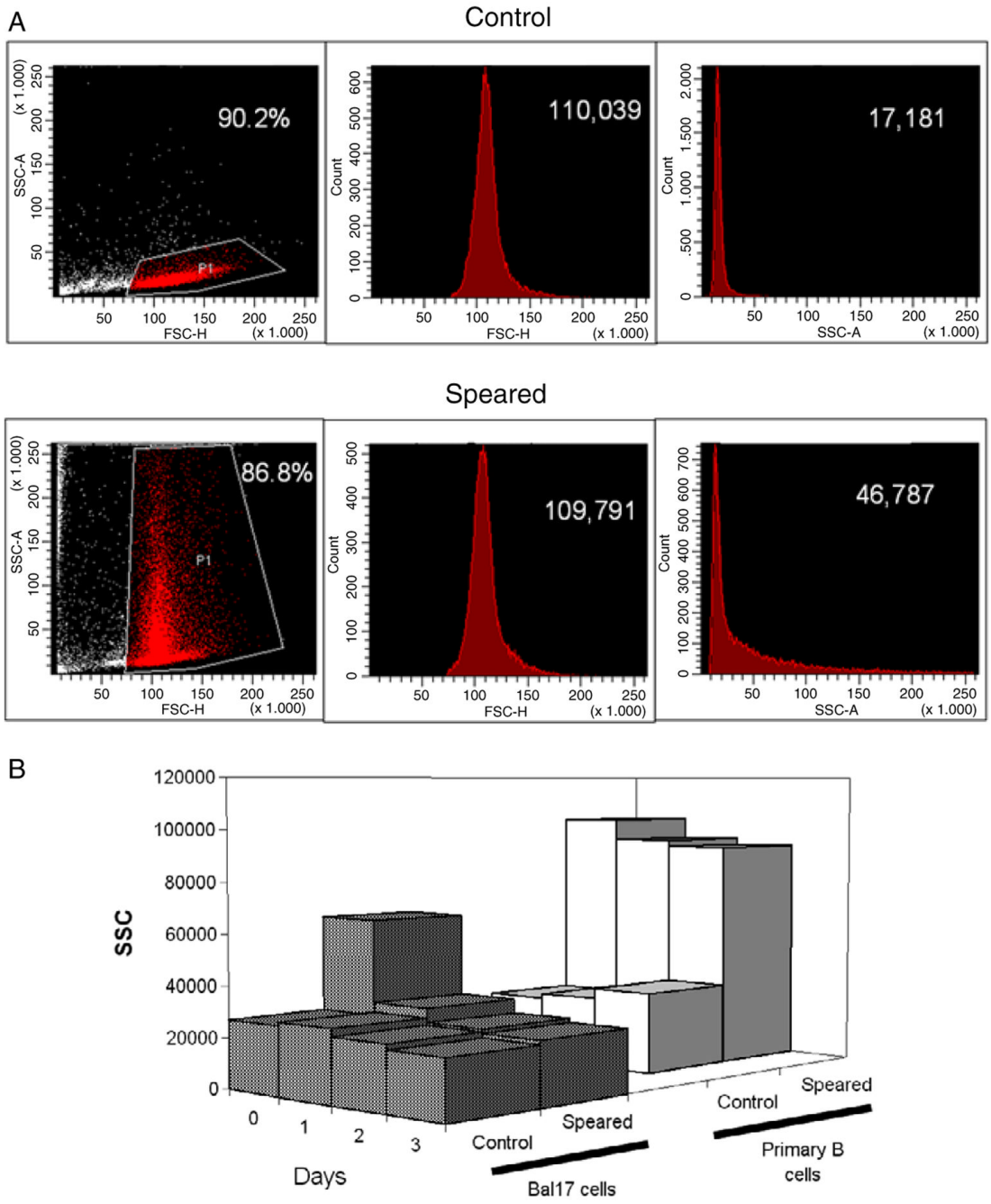

Figure 3.

Flow cytometry of CNT associated cells. (a) Speared primary B cells exhibit enhanced SSC. Scatter plots (left) show the recordings of FSC and SSC from 15 000 cells. The healthy cells were gated (grey (red online)) in the scatter plot and similar percentages in the total control and speared cells were compared. The histograms of FSC (middle) and SSC (right) of the selected populations are shown with the average values. (b) SSC have different transients in CNT associated primary B cells and Bal17 cells over the culture periods. Cells were speared with 0.4 fmol (a) and 1.6 fmol (b) CNTs.

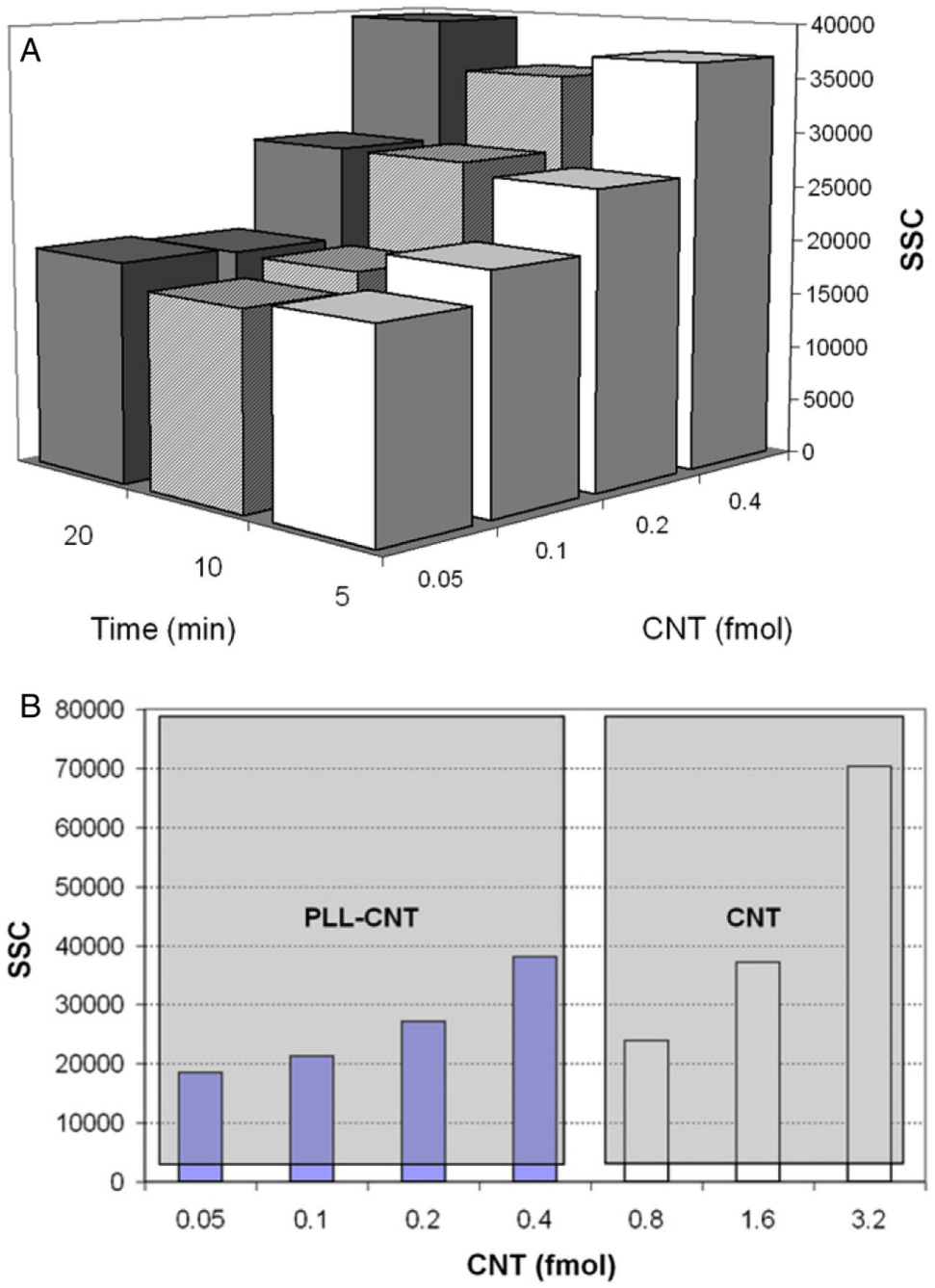

Figure 4.
SSC corresponding to CNT amount, the spearing time (a), and PLL modification of CNT (b). Each data point was obtained from 15 000 primary B cells.

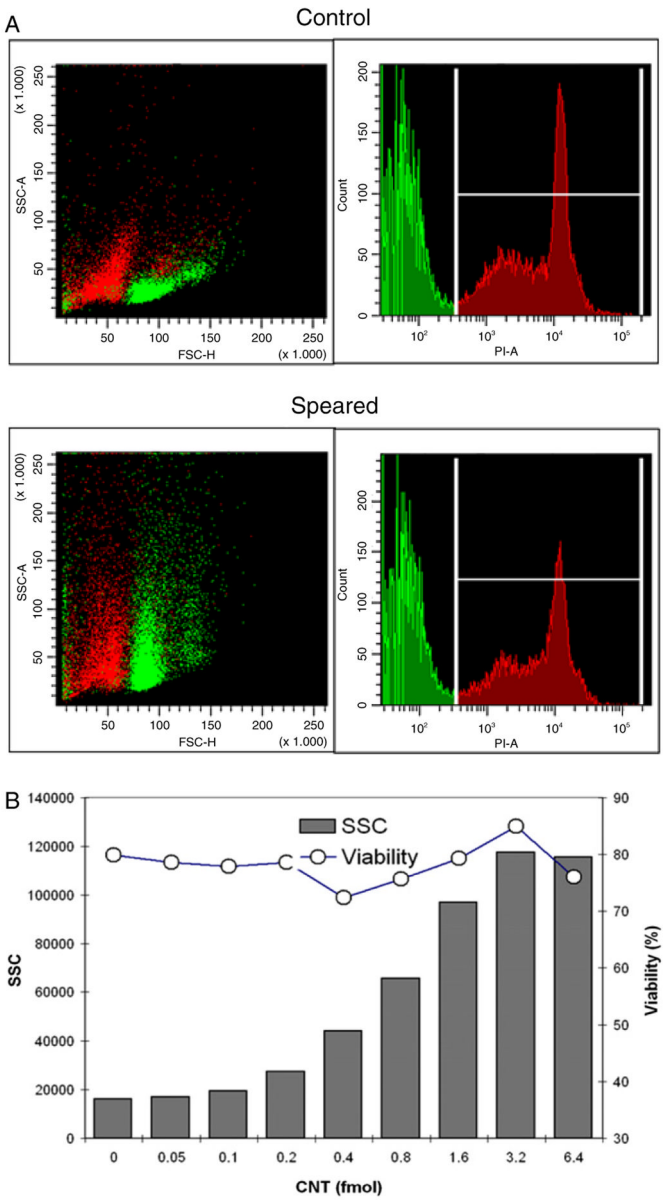

Figure 5.

The viability of CNT associated primary B cells and the SSC dose response to PLL–CNT amount. (a) The population correlation between SSC–FSC scatter plots (left) and PI histograms (right). Each figure represents recordings from 15 000 cells. (b) The dose response of SSC (column) and the cell viability (line) versus PLL–CNT amount. Each data point was extracted from 15 000 primary B cells.

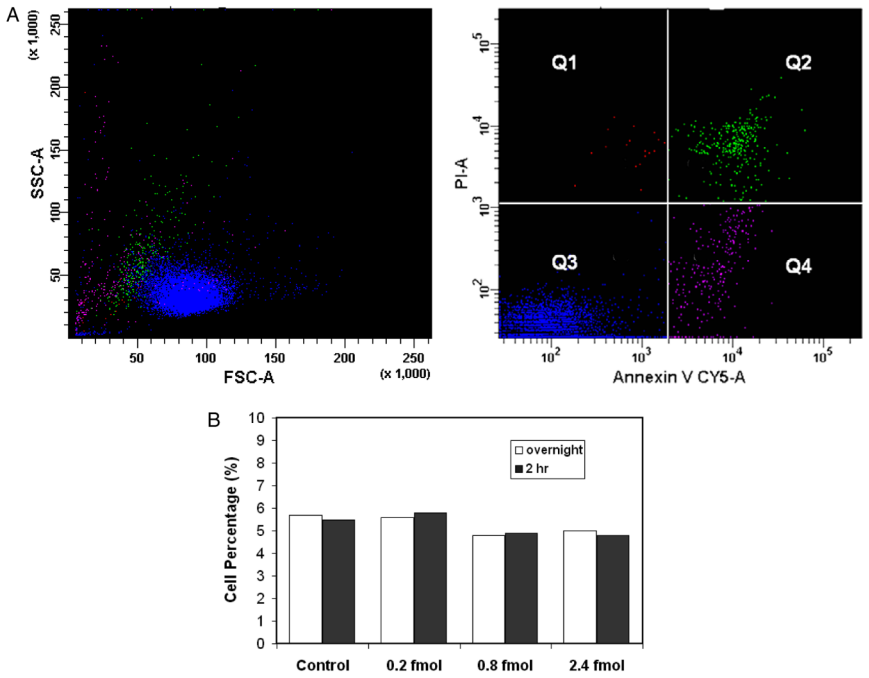

Figure 6.

Apoptosis assay with Annexin V and propidium iodide in Bal17 lymphoma cells. The cells were treated at three CNT dosages, i.e. 0.2 and 0.8 and 2.4 fmol. The assays were taken at 2 h of incubation after the association. The scatter plots (a) shows data from cells associated with 0.8 fmol CNTs and incubated overnight. The SSC and FSC of each population is shown correspondingly (left). The number in each portion represents the percentage of the cells. In (b), the percentages of cells in populations Q2 + Q4 (i.e. Annexin V positive) under various conditions were compared.

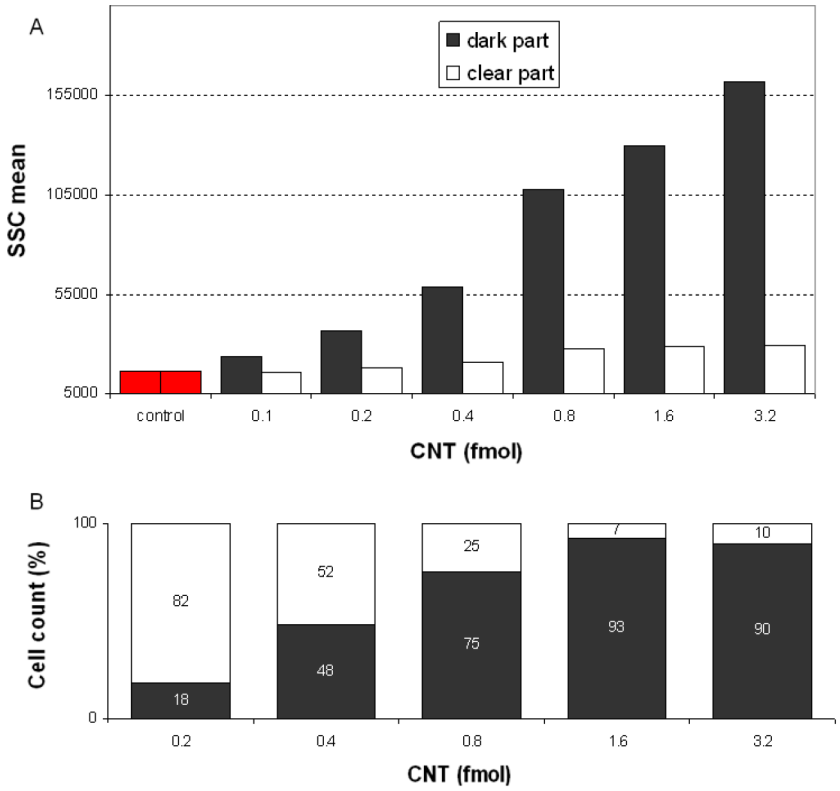

Figure 7.

Characterization of magnetically mediated cell separation. The average SSC levels (a) and cell percentage (b) of the dark and clear fractions yielded from the separation were plotted versus the amount of CNTs associated to cells. In (a), each data point was recorded from 15 000 primary B cells.

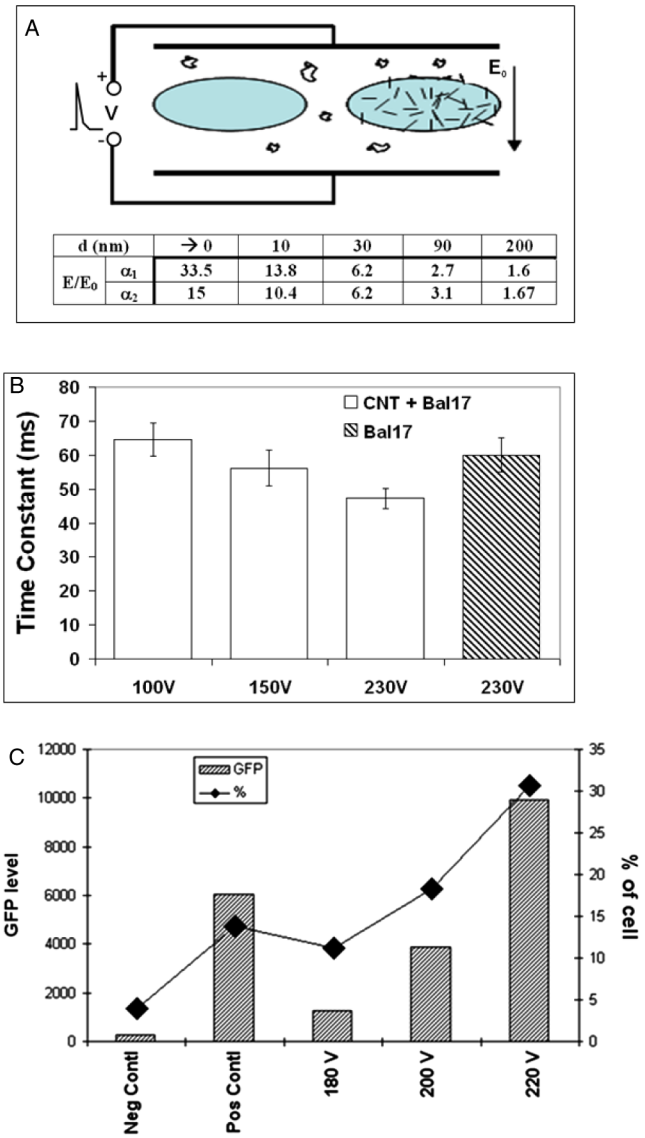

d (nm)		→ 0	10	30	90	200
E/E_0	α_1	33.5	13.8	6.2	2.7	1.6
	α_2	15	10.4	6.2	3.1	1.67

Figure 8.

Electric field enhancement by CNT in electroporation. (a) Sketch of electroporation with CNT-free (left) and CNT associated cells (right). Table insert: theoretical electric field (E) enhancement over the applied field (E_0) by a nanotube of 1 μm long. d denotes the distance to nanotube tip. a_1 and a_2 are the aspect ratios (i.e. diameter/length) of nanotubes, and equal to 0.1 and 0.5 respectively. (b) Electroporation time constants versus the voltages. A series of time constants of the CNT associated Bal17 cells were obtained under various voltages. They were compared to the time constant of regular Bal17 cells at 230 V. (c) Improvement of EGFP transfection by CNT mediated electroporation in Bal17 cells. The gates of EGFP positive cells were adjusted based on the *Neg Contl* and *Pos Contl*. The mean values of EGFP levels (left axis) and the percentages (right axis) of gated viable cells are shown. *Neg Contl*: negative control, cells speared and electroporated without plasmid; *Pos Contl*: positive control, cells without spearing and electroporated at 230 V with EGFP plasmid; 180, 200 and 220 V: CNT associated cells and electroporated with EGFP plasmids at corresponding voltages.

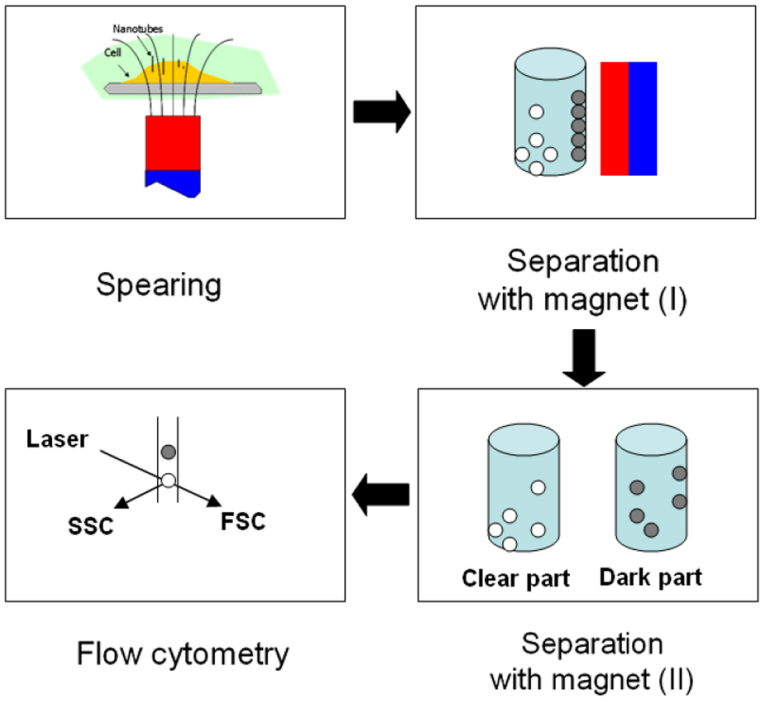

Scheme 1.
Magnetic field-mediated CNT–cell association and the characterization with flow cytometry.